Supplementary Information for

2D Mo_2AlB_2 Transition-Metal-Aluminum-Boride-Phase Integrated TiO_2 Nanoparticles Produce an Accelerated Carbendazim Photodegradation: Impact of Ohmic Junction and Electric Fields

Moorthy Gnanasekar Narendran [1], and Aruljothy John Bosco [1]*

[1] Advanced Materials Chemistry Laboratory, Department of Chemistry, Faculty of Engineering and Technology, SRM Institute of Science and Technology, Kattankulathur – 603 203, Chengalpattu, Tamil Nadu, India.

[*] Corresponding author information: Aruljothy John Bosco: E-mail: johnbosa@srmist.edu.in, sambosco@gmail.com. Tel: +91-98407 57430.

1. Characterization details

The crystallinity of the prepared catalysts was determined using X-ray diffraction (XRD) patterns on Bruker d8 advance XRD instrument equipped with a Cu Kα radiation (l = 1.5406) source. The microstructure and morphology of structural applications were evaluated using HRTEM (JEOL, JEM-2100f) and HRSEM (Thermo Scientific Apreo). The X-ray photoelectron spectroscopy (PHI VersaProbe 4 (XPS) Microprobe with Al Kα radiation source) was used to analyze sample surface characteristics. The carbon tape was utilized as a standard to calibrate the binding energy of XPS results. The UV-vis spectra were collected using a Shimadzu UV 3600i Plus spectrophotometer at room temperature. Raman spectra were collected using a HORIBA scientific spectrometer with a 534 nm laser (LabRAM HR Evolution, Horiba.). The FTIR spectra were recorded using a Shimadzu IRTracer-100. The surface textural characterization was determined by the BET and BJH method of the N_2 adsorption-desorption isotherms using a Quantachrome Autosorb IQ. PL measurements were collected in the FLS1000 (Edinburgh Instruments) spectrometer. An OrigaLys electroflex electrochemical workstation was used to conduct EIS, photocurrent, and Mott-Schottky analysis using a three-electrode system of glassy carbon, Ag/AgCl, and Platinum electrodes 0.1 mol L^{-1} Na_2SO_4 electrolyte (pH≈6). The photocurrent analysis was measured in a 1.5 AM Photo Emission Tech solar simulator with a 10-second on-off cycle. The working electrodes were prepared by sonicating catalysts in ethanol with 5 µL 10 wt.% Nafion for 30 min. The resulting sludge was then air-dried after a slowing drop cast on a glassy carbon electrode. The current-voltage (I-V) characteristics were measured using a two-electrode system (counter

electrode and working electrode). The slurry was formed by sonicating a 5 mg sample in 1 mL of ethanol. The slurry was then injected into the space between the two conducting surfaces of FTO glasses (0.5 × 0.5 cm^2). The two FTO glasses were sealed using polyvinyl acetate. The entire preparation procedure was carried out in a glove box. The ESR spectrometer JEOL JES-FA200 (X-band frequency 8.75-9.65 GH) was used to measure the ESR spectra.

2. Photocatalyst test

Photocatalytic degradation of CBZ in aqueous solution under simulated sunlight (300W xenon lamp, AM 1.5G). In a typical degradation test, a catalyst was dispersed in 40 mL CBZ aqueous solution and then kept in dark condition for 30 min for adsorption-desorption equilibrium. At regular intervals, 3 mL solution was collected and centrifuged, Then the concentration of residual CBZ in the reaction solution was immediately determined by UV-visible spectrophotometer at a wavelength of 286 nm.

$$Degradation\ efficiency\ (\%) = (1 - C_0/C) \times 100 \quad \textbf{(1)}$$

The initial and remaining concentrations of CBZ in the solution, denoted as C_0 and C (both in ppm), respectively, were measured in triplicate for each experimental set. The reported results represent the average of these triplicates, with error bars indicating the reproducibility of data across repeated experiments. The primary oxidative species identified through trapping experiments included $^{\bullet}O_2^-$, $^{\bullet}OH$, electrons, and holes, detected using BQ, IPA, $AgNO_3$, and TEOA, respectively. Furthermore, the rate constants for CBZ degradation on TiO_2 and its composite were determined using the first-order kinetics equation demonstrated by the Langmuir-Hinshelwood mechanism.

$$ln(C_0/C) = Kt \quad \textbf{(2)}$$

C_0 is the initial concentration of CBZ, C is the concentration at the time t and K is the rate constant of the reaction.

3. Computational method

The work functions of TiO_2 and Mo_2AlB_2 were calculated using openMX ver. 3.9 [1]. The band structure and density of states were computed using the CP2K package[2], utilizing the generalized gradient approximation (GGA) with the Perdew and Wang 1991 (PW91) functional (GGA-PW91). Parameters such as the energy cut-off, self-consistent field (SCF) tolerance, and k-point values were meticulously set to 550 eV, 1 × 10^{-5} eV $atom^{-1}$, and 3 × 2

× 3, respectively. Norm-conserving pseudo-potentials for the ionic cores were employed to enhance transferability and reduce the number of plane waves needed to represent the Kohn-Sham orbitals. The optimized structures of tetragonal TiO_2, with lattice constants a=b=3.77 Å, and c= 9.43 Å, and Orthorhombic Mo_2AlB_2, with lattice constants a=3.07 Å, b= 11.5 Å, and c=3.18 Å, are illustrated in Fig. S1. These structural details provide a foundation for further analysis and understanding of the material's electronic properties and behavior.

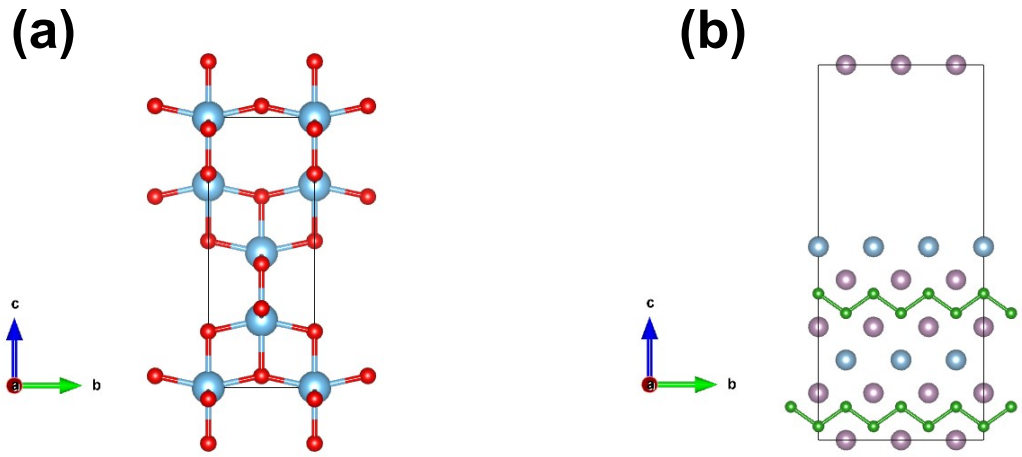

Fig. S1 The optimized structures of tetragonal TiO_2 (a), and orthorhombic Mo_2AlB_2 (b).

The Raman spectra were carried out for MoAlB, Mo_2AlB_2, and the Fukui function of CBZ using the Gaussian 16 program with the B3LYP method, and 6-31G* basis set[3]. By examining the frontier electron densities of the HOMO and LUMO orbitals, we identified potential reaction sites vulnerable to attacks by reactive species within the catalytic system. Additionally, the Fukui function, a key concept in conceptual density functional theory, was utilized to predict electrophilic, nucleophilic, and radical attack sites. This method has proven valuable in forecasting the regioselectivity of reactions across various systems.

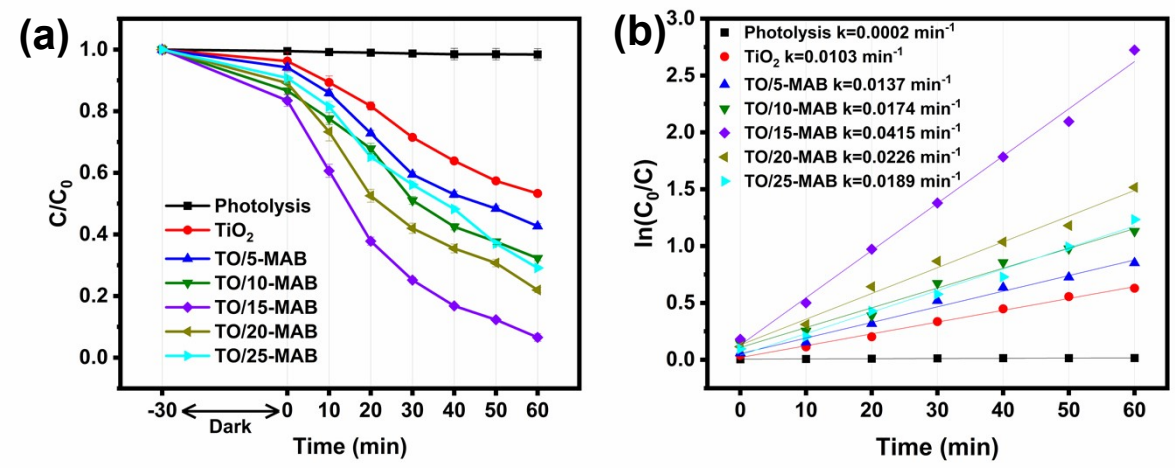

Fig. S2 CBZ photodegradation efficiency of different catalysts under optimized conditions (a). Kinetics study for all the catalysts (b).

Table S1 Summary of photocatalytic carbendazim degradation over the different catalysts.

Catalyst	Catalyst dosage (mg)	Pollutant concentration (mg/L)	Light source	Degradation % (Time)
TiO_2/Mo_2AlB_2 (This Work)	15	15	AM1.5 300 W Xenon Lamp	93.4% (60 min)
$SrTiO_3/Mo_2AlB_2$[4]	20	10	Halogen Lamp 500 W (Crompton)	87.5% (80 min)
$CoTiO_3/CaTiO_3$[5]	25	15	300 W Xenon Lamp >420 nm	89% (60 min)
$Gd_2(WO_4)_3$[6]	60	10	Philips projection Lamp (250 W, 532 nm))	98% (140 min)
$Bi_2S_2/BiFeO_3$[7]	50	10	Xenon (150 W, >400 nm)	95% (120 min)
$Cu_2O/ZnO@PET$[8]	32	1	UV, T=52 ºC	98.1% (160 min)
BiOBr[9]	40	20	Metal Halide (300 W)	99% (150 min)
$Gd_2S_3/NRGO$[10]	20	100	Xenon Lamp	94% (80 min)
Fe/TiO_2[11]	1000	8	Sunlight, T=25 ºC	98% (60 min)
α-Fe_2O_3/β-CD-CNFs[12]	50	5×10^{-5} M	-	93.5% (120 min)

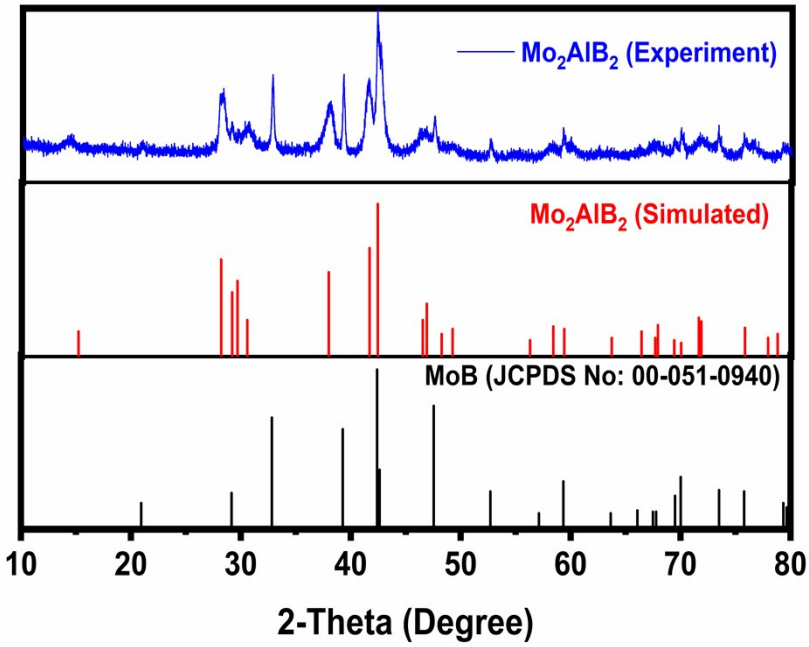

Fig. S3 Comparison of XRD pattern of Mo_2AlB_2 with experimental, simulated stick patterns of Mo_2AlB_2 and standard MoB Stick patterns.

Table S2 Calculated Crystallite size and Lattice strain of bare TiO_2 and TO/15-MAB composite.

Sample code	2-Theta (Degree)	Crystallite size (nm)	Lattice strain (%)
Bare TiO_2	25.583	34.4	0.471
TO/15-MAB composite	25.437	22.7	0.709

Table S3 The calculated phonon lifetime (in ps) of bare TiO_2 and TO/15-MAB composite using Raman spectra. (Reduced Planck's constant $\hbar = 5.3 \times 10^{-12}$ cm^{-1} s)

Sample name	1st E_g Raman mode	B_{1g} Raman mode	A_{1g}, B_{1g} Raman mode	E_g Raman mode
Bare TiO_2	349.3	200.6	188.8	155.2
TO/15-MAB composite	346.3	191	172.1	155.1

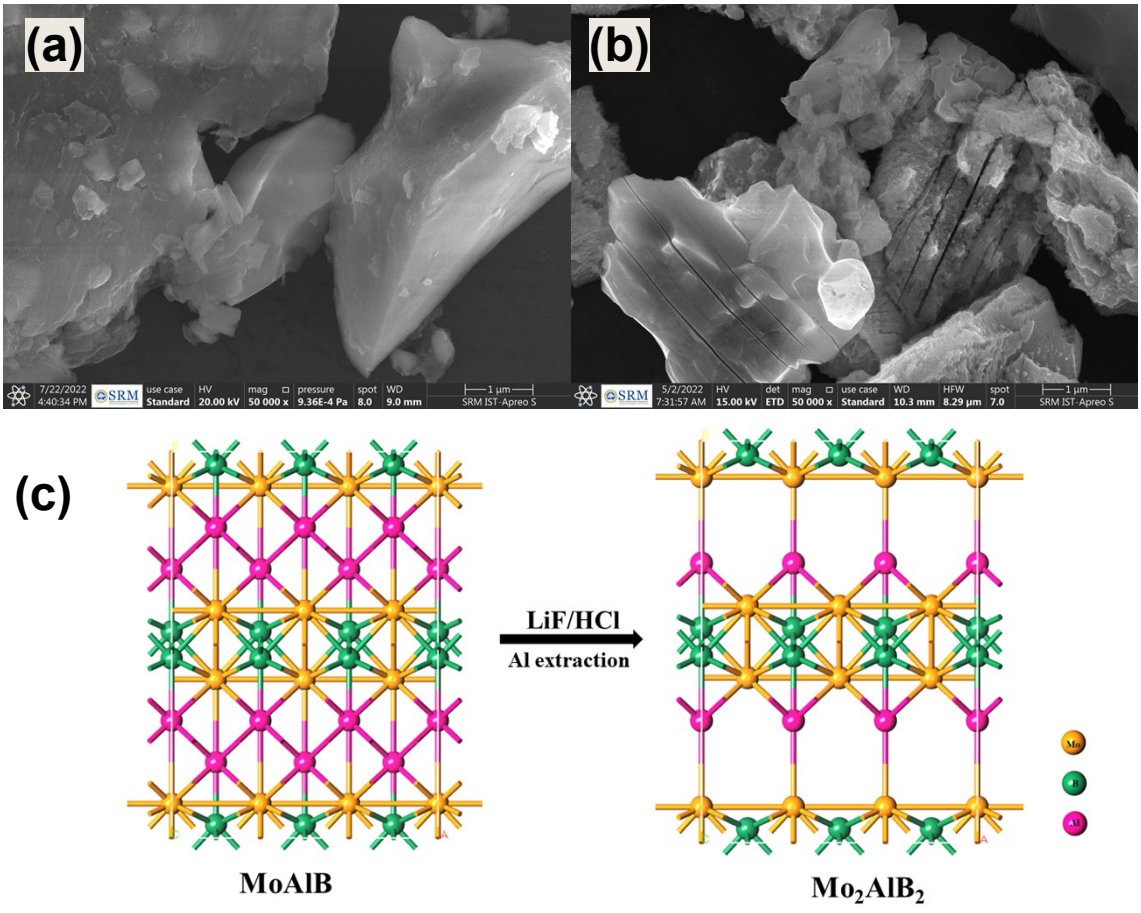

Fig. S4 HRSEM images of MoAlB before (a) and after (b) the etching process. Schematic structure of removal Al from MoAlB to form Mo_2AlB_2 using LiF/HCl (c).

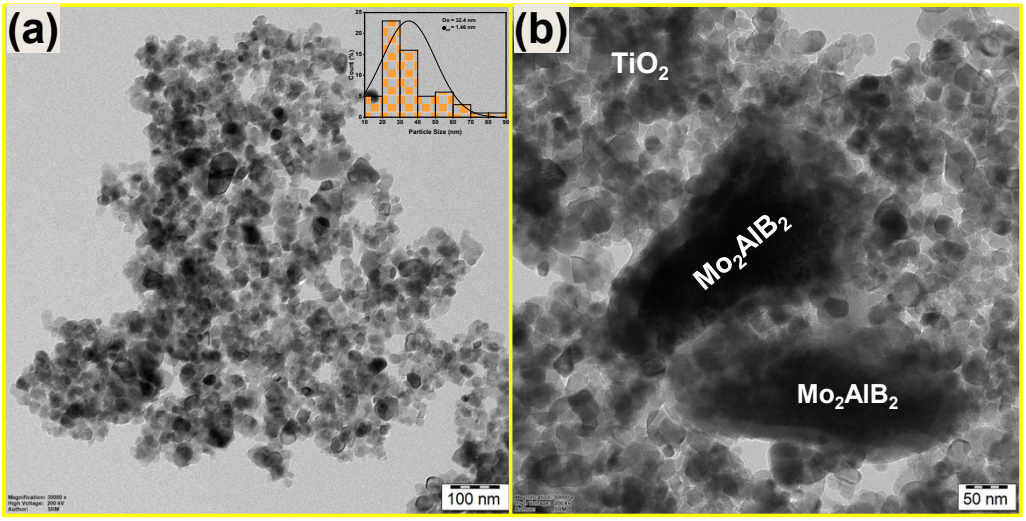

Fig. S5 HRTEM image of bare TiO_2 with the average particle size distribution curve (a) and Inside (a). HRTEM image of TO/15-MAB composite (b).

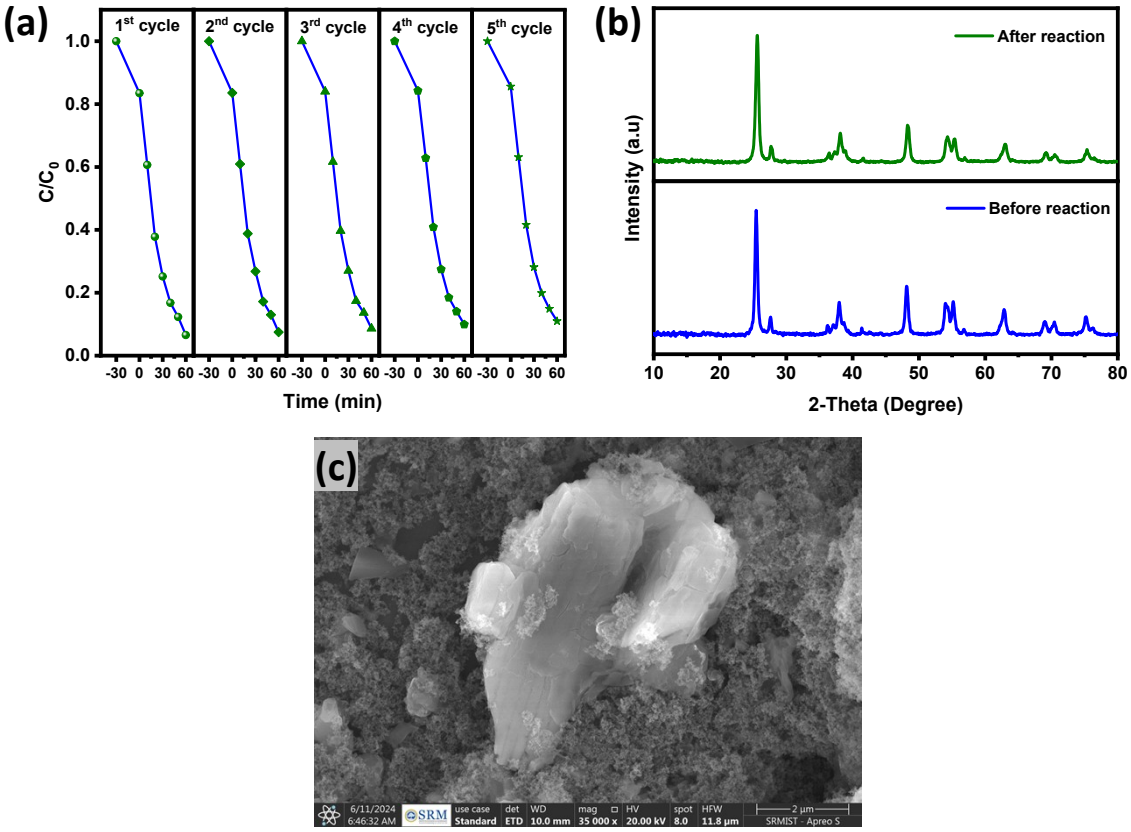

Fig. S6 Consecutive cycles of the CBZ photodegradation in the presence of TO/15-MAB (a). XRD patterns of TO/15-MAB before and after the reaction (b). HRSEM image of TO/15-MAB after 5 cycles (c).

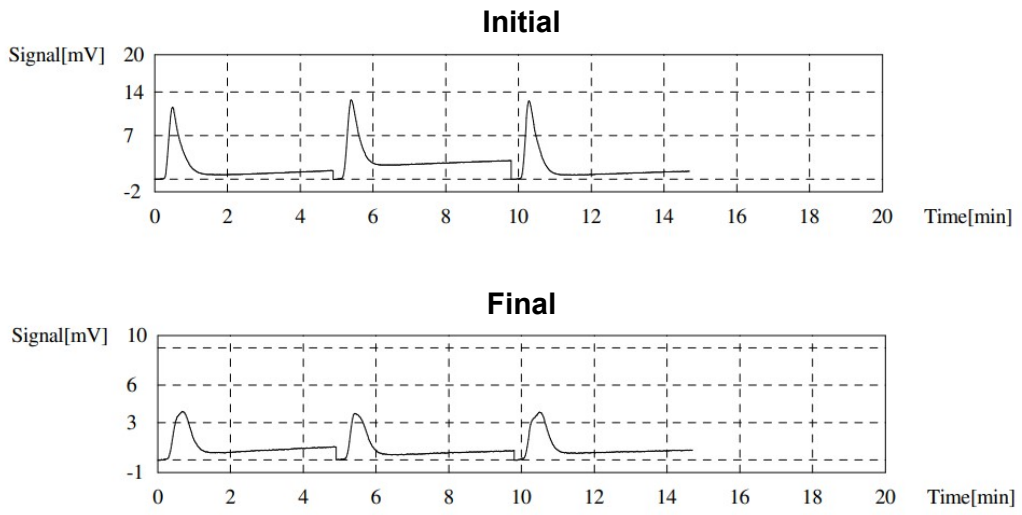

Fig. S7 TOC signals of carbendazim before and after photocatalysis using TO/15-MAB composite.

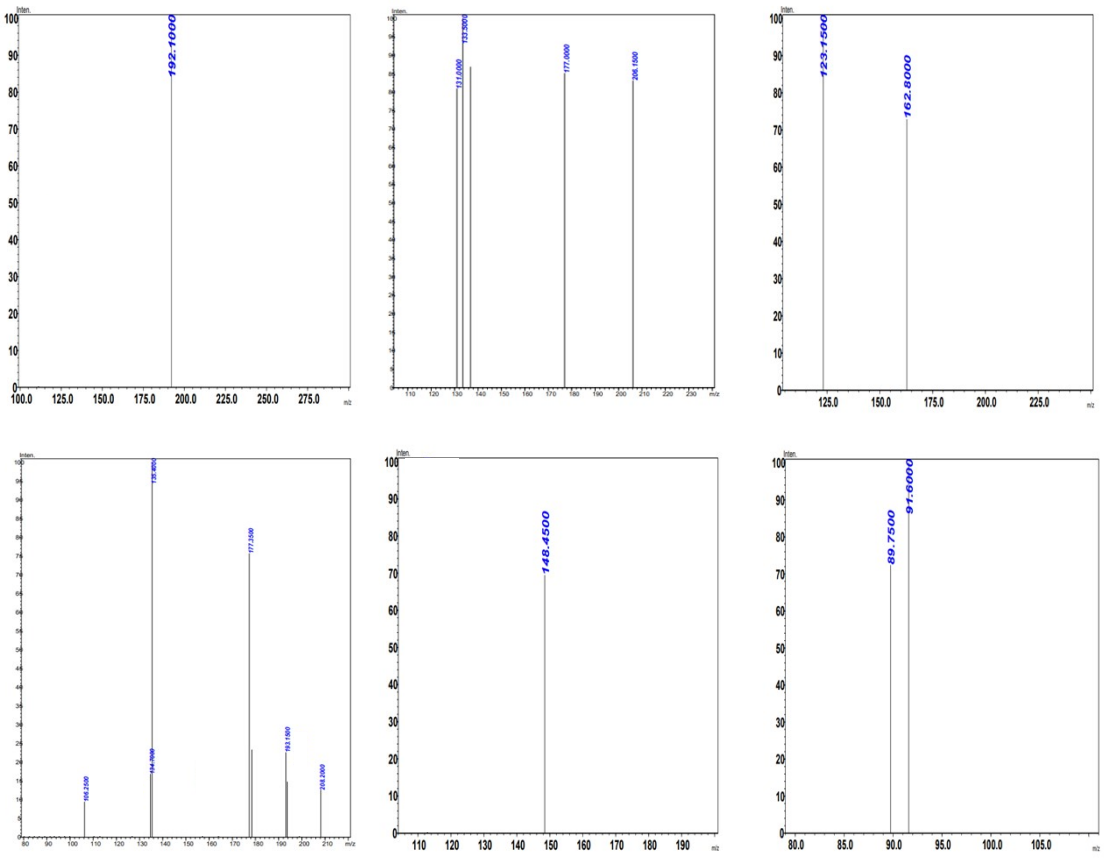

Fig. S8 Fragment ions and oxidation products in the identification of CBZ in the catalytic system by LCMS.

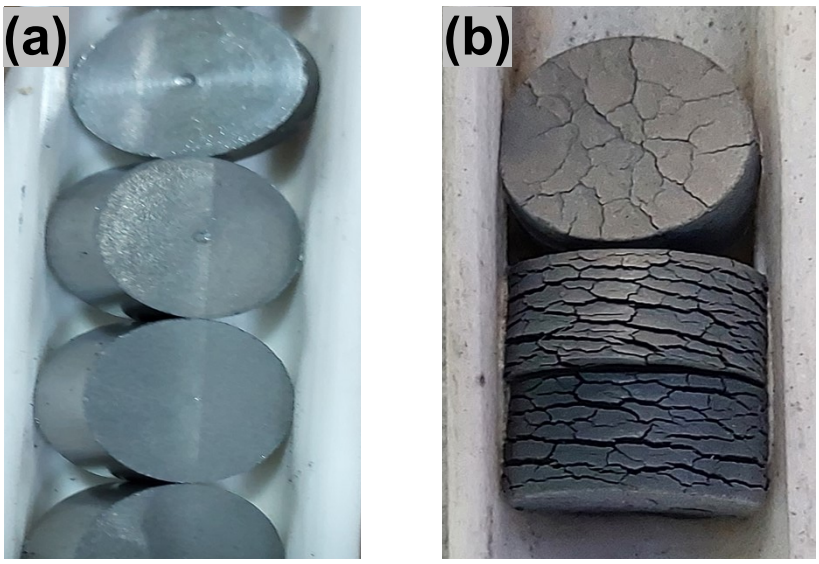

Fig. S9 Photo of MoAlB before (a) and after heating (b).

4. Impact of MoAlB cocatalyst in photocatalysis

The synthesized Mo_2AlB_2 contains an impurity of MoAlB. This impurity plays a crucial role as a cocatalyst in the TiO_2 composites, particularly in the context of carbendazim degradation. Despite the assessment of synthesized Mo_2AlB_2's photocatalytic activity, the degradation efficiency of the TiO_2/MoAlB composite was found to be 73.4%, which is 1.25 times lower than that of the TiO_2/Mo_2AlB_2 composite, although it does show improvement over bare TiO_2 (Fig. S10a). Several important factors contribute to this discrepancy.

1. **Higher Work Function of MoAlB:** The higher work function of MoAlB leads to the formation of a Schottky junction when combined with TiO_2, as opposed to the Ohmic junction created with Mo_2AlB_2. This distinction influences charge carrier dynamics, potentially resulting in less efficient charge separation and transport in the MoAlB composite (Fig. S10b).

2. **Enhanced Light Absorbance:** Mo_2AlB_2 exhibits superior light absorbance properties compared to MoAlB. This increased light absorption enhances the generation of electron-hole pairs, which are crucial for effective photocatalytic degradation processes (Fig. S10c).

3. **Surface Area and Pore Volume:** Mo_2AlB_2 possesses a higher surface area and pore volume than MoAlB, providing more active sites for photocatalytic reactions. This

structural advantage allows for improved interaction with pollutants, facilitating more efficient degradation (Fig. S10(d and e)).

While the TiO_2/MoAlB composite showed reduced photocatalytic activity compared to TiO_2/Mo_2AlB_2, the Schottky junction formed by MoAlB impurity may still play a minor role in charge separation, which could contribute to the overall performance of the composite as discussed in the Introduction section.

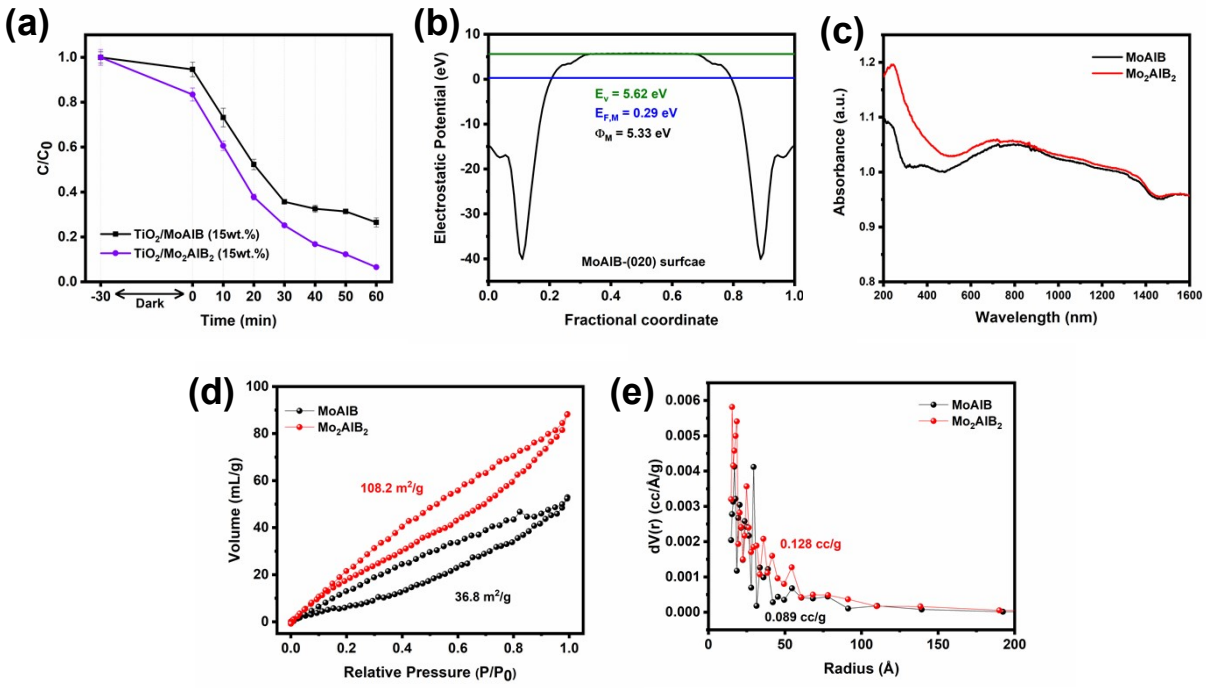

Fig. S10 CBZ photodegradation efficiency of TiO_2/MoAlB and TiO_2/Mo_2AlB_2 composites (a), Average potential profile along the Z-axis direction for MoAlB (b), UV DRS spectra of MoAlB and Mo_2AlB_2 (c), BET N_2-sorption isotherm and pore volume plots of MoAlB and Mo_2AlB_2 (d-e).

References

1 S. Boker, M. Neale, H. Maes, M. Wilde, M. Spiegel, T. Brick, J. Spies, R. Estabrook, S. Kenny, T. Bates, P. Mehta and J. Fox, OpenMx: An Open Source Extended Structural Equation Modeling Framework, *Psychometrika*, 2011, **76**, 306–317.

2 J. P. Perdew, M. Ernzerhof and K. Burke, Rationale for Mixing Exact Exchange with Density Functional Approximations, *J. Chem. Phys.*, 1996, **105**, 9982–9985.

3 M. J. Frisch, G. W. Trucks, H. B. Schlegel, G. E. Scuseria, M. a. Robb, J. R. Cheeseman, G. Scalmani, V. Barone, G. a. Petersson, H. Nakatsuji, X. Li, M. Caricato, a. V Marenich, J. Bloino, B. G. Janesko, R. Gomperts, B. Mennucci, H. P. Hratchian, J. V Ortiz, a. F Izmaylov, J. L. Sonnenberg, Williams, F. Ding, F. Lipparini, F. Egidi, J. Goings, B. Peng, A. Petrone, T. Henderson, D. Ranasinghe, V. G. Zakrzewski, J. Gao, N. Rega, G. Zheng, W. Liang, M. Hada, M. Ehara, K. Toyota, R. Fukuda, J. Hasegawa, M. Ishida, T. Nakajima, Y. Honda, O. Kitao, H. Nakai, T. Vreven, K. Throssell, J. a. Montgomery Jr., J. E. Peralta, F. Ogliaro, M. J. Bearpark, J. J. Heyd, E. N. Brothers, K. N. Kudin, V. N. Staroverov, T. a. Keith, R. Kobayashi, J. Normand, K. Raghavachari, a. P Rendell, J. C. Burant, S. S. Iyengar, J. Tomasi, M. Cossi, J. M. Millam, M. Klene, C. Adamo, R. Cammi, J. W. Ochterski, R. L. Martin, K. Morokuma, O. Farkas, J. B. Foresman and D. J. Fox, 2016, Gaussian 16, Revision C.01, Gaussian, Inc., Wallin.

4 M. G. Narendran, S. Peters, A. John Bosco, G. Keerthiga, B. Neppolian, S. M. Senthil Kumar and T. Xiaoteng Liu, Pioneering Exploration of Mo_2AlB_2-Transition-Metal-Aluminum-Boron-Phase-Supported Hydrophobic $SrTiO_3/Mo_2AlB_2$ Nanocomposite for Improved Photocatalytic Carbendazim Degradation and CO_2 Reduction to Ethanol through the Schottky Junction, *Solar RRL*, 2024, **8**, 2301043.

5 M. G. Narendran, E. Vijayakumar, M. Govinda Raj, R. Preetha, J. John Alphin, R. Mahaan, B. Neppolian and A. John Bosco, Shining a Light on Fungicide- Water: Enhanced Photocatalytic Degradation Using the $CoTiO_3/CaTiO_3$ Nanocomposite and Experimental and Theoretical Viewpoints on Improved Intervalence Charge Transfer from O^{2-} to Ti^{4+} and from Co^{2+} to Ti^{4+} Ions and Spatial Charge Transfer, *New J. Chem.*, 2024, **48**, 6109–6123.

6 S. Periyasamy, J. Vinoth Kumar, S. M. Chen, Y. Annamalai, R. Karthik and N. Erumaipatty Rajagounder, Structural Insights on 2D Gadolinium Tungstate Nanoflake: A Promising Electrocatalyst for Sensor and Photocatalyst for the Degradation of Postharvest Fungicide (Carbendazim), *ACS Appl. Mater. Interfaces*, 2019, **11**, 37172–37183.

7 Y. P. Bhoi, A. K. Nayak, S. K. Gouda and B. G. Mishra, Photocatalytic Mineralization of Carbendazim Pesticide by a Visible Light Active Novel Type-II $Bi_2S_3/BiFeO_3$ Heterojunction Photocatalyst, *Catal. Commun.*, 2018, **114**, 114–119.

8 L. Sh. Altynbaeva, M. Barsbay, N. A. Aimanova, Z. Ye. Jakupova, D. T. Nurpeisova, M. V Zdorovets and A. A. Mashentseva, A Novel Cu_2O/ZnO@PET Composite Membrane for the Photocatalytic Degradation of Carbendazim, *Nanomaterials*, 2022, **12**, 1724.

9 H. Wang, G. Shi, G. Wang, R. Wang, W. Chen, J. Li, Y. Wei and Y. Zhang, Investigation on the Photocatalytic Degradation Properties of BiOX on Carbendazim and Its Mechanism, *ChemistrySelect*, 2023, **8**, e202204707.

10 K. Yogesh Kumar, M. K. Prashanth, L. Parashuram, B. Palanivel, F. A. Alharti, B. H. Jeon and M. S. Raghu, Gadolinium Sesquisulfide Anchored N-Doped Reduced Graphene Oxide for Sensitive Detection and Degradation of Carbendazim, *Chemosphere*, 2022, **296**, 134030.

11 T. Kaur, A. Sraw, A. P. Toor and R. K. Wanchoo, Utilization of Solar Energy for the Degradation of Carbendazim and Propiconazole by Fe Doped TiO_2, *Solar Energy*, 2016, **125**, 65–76.

12 N. Sebastian, W.-C. Yu, D. Balram, F. S. Al-Mubaddel and M. Tayyab Noman, Functionalization of CNFs Surface with β-Cyclodextrin and Decoration of Hematite Nanoparticles for Detection and Degradation of Toxic Fungicide Carbendazim, *Appl. Surf. Sci.*, 2022, **586**, 152666.